PAPER

Tuning nanoparticles' internal structure: fluorinated single-chain nanoparticles (SCNPs) generated by chain collapse of random copolymers†

Marah Alqaisi, [ID] [a] Justus F. Thümmler, [ID] [a] Florian Lehmann, [ID] [b]
Franz-Josef Schmitt, [c] Leonie Lentz, [c] Fabian Rieder, [ID] [c] Dariush Hinderberger [ID] [b]
and Wolfgang H. Binder [ID] *[a]

The generation of nanosized compartments in single chain nanoparticles (SCNPs) is a promising approach to generate individualized confinement-zones on a small scale for drug-encapsulation or catalysis. We here report the synthesis and characterization of compartmented, fluorinated SCNPs generated by single-chain collapse of amphiphilic copolymers. Polyethylene glycol (PEG) functionalized monomers were utilized as hydrophilic moieties, while hydrophobic residues were introduced using different mole fractions of either aliphatic or fluorinated monomers. Single chain collapse and subsequently crosslinking via copper-catalyzed azide−alkyne click reactions in selective and non-selective solvents yields internally structured SCNPs with hydrodynamic radii of 2.5−5.8 nm. All of the SCNPs exhibited water solubility, but displayed different compartmentations sized <1 nm, depending on the type of hydrophobicity and the monomer ratio. Investigations using continuous wave electron paramagnetic resonance and decay associated fluorescence spectroscopy, specifically targeting the hydrophobic cores of the SCNPs, revealed significant differences between the aliphatic and fluorinated cores of the SCNPs as probed by different specific molecular labels, finally allowing specific embedding of molecules into the specific compartments.

Introduction

In nature a variety of non-covalent interactions, encompassing a spectrum of attractive and repulsive forces, are employed to arrange molecules into complex assemblies, often with a remarkable degree of order.[1,2] Thus the self-assembly of polymers in solution generates well-known assemblies such as block-copolymeric micelles, primarily guided by incompatibilities between the polymer blocks and the surrounding solvent molecules, in addition to supramolecular inter/intrachain interactions within the polymer segments.[3–6] Collapsing single

polymer chains in interaction with surrounding solvent molecules results in single-chain nanoparticles (SCNPs), where the interplay of forces (intermolecular and intramolecular solvent/polymer and polymer/polymer interactions) generates nanoparticles in dimensions of a single polymer chain. If the so-generated assemblies are fixed by crosslinking the collapsed chain, such SCNPs can offer unique advantages for various applications, such as in catalysis[7–11] and sensing,[12,13] as well as in nanomedicine and drug delivery.[14–17] It is exciting to note that the imperfect confinement of such a collapsed polymer chain bears resemblance to intrinsically disordered proteins (IDP),[18,19] where a delicate balance between disorder and order gives rise to compartmentalized, sometimes highly organized assemblies (i.e. protein fibers).[20] The size and morphology of such SCNPs depend on many factors such as the chosen crosslinking chemistry and the subsequent density and the initial conditions of chain collapse. Thus, intra-chain crosslinking is crucial in preserving the compactness of the polymer chain in addition to the length of the crosslinker to control the final shape of the nanoparticle. It has been shown that short crosslinkers induce predominantly short-range loops along the polymer chain, leading to less compacted ellipsoid-shaped SCNPs.[21,22] Crosslinking chemistries for single-

[a]Macromolecular Chemistry, Institute of Chemistry, Faculty of Natural Science II (Chemistry, Physics and Mathematics), Martin-Luther-University Halle-Wittenberg, von-Danckelmann-Platz 4, Halle D-06120, Germany.
E-mail: wolfgang.binder@chemie.uni-halle.de
[b]Physical Chemistry, Institute of Chemistry, Faculty of Natural Science II (Chemistry, Physics and Mathematics), Martin-Luther-University Halle-Wittenberg, von-Danckelmann-Platz 4, D-06120 Halle, Germany
[c]Institute of Physics, Faculty of Natural Science II (Chemistry, Physics and Mathematics) Martin Luther University Halle-Wittenberg, von-Danckelmann-Platz 3, D-06120 Halle, Germany

chain collapse are manifold, among them irreversible covalent, reversible covalent (dynamic) or noncovalent chemical bonds, all of which affect the final properties of the produced particles as well as the overall structure.[23] Next to the crosslinking chemistry, which is used to fix the SCNP in its collapsed state, the design of the initial copolymer is responsible for the SCNPs' nanostructure.[24] The use of amphiphilic copolymers promotes the formation of internal structures, such as Janus-shapes or core–shell structures,[25] which can further be used to encapsulate e.g. drugs or catalysts, improving their function and efficiency. We have recently reported the synthesis of water-soluble, amphiphilic SCNPs with defined internal hydrophobic compartments, displaying hydrodynamic radii of 4–5 nm, bearing compartments which are generated during collapse of the polymer chain in a selective solvent.[26] Those SCNPs can selectively be loaded with different labels, then situated inside the SCNPs' internal structure. When collapsed in water as a selective solvent, those labels experience a well-defined, hydrophobic, and dense surrounding inside the core of the SCNPs, whereas THF as a nonselective solvent produces more sparse, less defined structures in which the hydrophobic compartments are positioned in multiple regions distributed across the particle in a sparse structure.[27] A similar pathway, dependent on the assembly/collapse process leading to compartmentation was observed by Delledonne et al.[28] reporting the formation of unimer micelles serving as carriers for a fluorescent dye for biological applications. A random copolymer, composed of hydrophilic/hydrophobic segments, then generated small unimolecular micelles (<10 nm), featuring a hydrophobic fluorinated core formed through hydrophobic/hydrophilic interactions in water. As no covalent crosslinking was introduced the embedding of a hydrophobic fluorescent dye was accomplished dynamically within the hydrophobic core once dissolved in a nonselective solvent. Ko et al.[29] reported the formation of well-defined nanoparticles from folding a single amphiphilic fluorous random copolymer for encapsulating a fluorinated agrochemical. In a similar fashion, Koda et al.[30,31] produced biocompatible amphiphilic random copolymers, with PEG chains and per-fluorinated alkane pendants, based on hydrophilic/hydrophobic interactions to generate multi-chain micellar aggregates in addition to single-chain unimer micelles bearing a hydrophilic shell and a fluorinated hydrophobic compartment in water. Matsumoto et al.[32] produced double-core or multicompartment micellar morphologies from orthogonal folding and self-assembly of fluorous/amphiphilic random block copolymers in water. Shibata et al.[33] reported the investigation of self-folding and self-assembly of amphiphilic random copolymers compromising hydrophilic PEG side chains (4.5 or 8.5 oxyethylene units) in addition to hydrophobic butyl or dodecyl pendants. It was revealed that the pendant design played an important role in inducing intramolecular self-folding or intermolecular self-assembly.

We here report on the synthesis and investigation of cross-linked, water-soluble, amphiphilic SCNPs featuring defined hydrophobic/hydrophilic monomer combinations together with different embedded internal compartments depending on the choice of the respective monomers. The hydrophobic entities are incorporated via either purely aliphatic or fluorinated monomer sidechains, representing the first report of core-crosslinked, fluorinated SCNPs, which have previously are known only as non-crosslinked unimolecular micelles. This design allows the SCNPs to adopt different compartments, guided by their hydrophilicity, hydrophobicity and fluorophilicity. The size/volume of both, the aliphatic/fluorinated and hydrophilic parts were controlled by varying the molar ratios of the monomers in the precursor copolymers. Using RAFT polymerization, we varied the content of the hydrophobic monomers ranging from 10 mol% to 30 mol% of the aliphatic or fluorinated monomer ratio in order to modulate compartment formation after chain collapse. To probe the influence of the additional fluorinated monomer on the final shape, morphology, size, and physicochemical properties of the SCNPs, chain collapse was conducted in two different solvents (water and THF). Several methods were used to reveal the nature of the so-formed SCNPs, such as size exclusion chromatography (SEC) and ^{1}H-diffusion-ordered nuclear magnetic resonance (^{1}H-DOSY NMR) spectroscopy, and we also focused on continuous wave electron paramagnetic resonance (CW-EPR) spectroscopy and decay associated fluorescence spectroscopy (DAS) confirming differences between the aliphatic and fluorinated compartments inside the SCNPs (see Scheme 1).

Experimental

Materials

2,2′-Azobis(2-methylpropionitrile) AIBN (98%, Sigma-Aldrich), 4-cyano-4-(dodecylsulfanylthiocarbonyl)sulfanylpentanoic acid CDPA (97%, abcr), poly(ethylene glycol)methyl ether methacrylate PEGMA (average M_n 300 Da, containing 300 ppm BHT as an inhibitor and 100 ppm MEHQ as an inhibitor, ≤100%, Sigma-Aldrich), butyl methacrylate BuMA (99%, containing monomethyl ether hydroquinone as an inhibitor, Sigma-Aldrich), 2,2,3,3,4,4,4-heptafluorobutyl methacrylate HFBMA (97%, containing MEHQ as an inhibitor, Sigma-Aldrich), chloroform-d CDCl$_3$ (stabilized with Ag, ≤100%, ARMAR), 1,7-octadiyne (98%, Sigma-Aldrich), copper(II) sulphate pentahydrate (≥99%, VEB Laborchemikalien), copper(I) bromide (98%, Sigma-Aldrich), (+)-sodium L-ascorbate (≥98%, Sigma-Aldrich), N,N,N′,N″,N″-pentamethyl diethylenetriamine PMDTA (99%, Sigma-Aldrich), deuterium oxide D$_2$O (99.9%, Sigma-Aldrich), 2,2′-bipyridine (≥99%, Sigma-Aldrich), 5-DOXYL stearic acid, ammonium salt 5-DSA (>99%, Avanti polar lipids). The chemicals were used as received if not mentioned otherwise. All monomers were passed through a column of basic aluminum oxide prior to use to remove the inhibitors and subsequently dried using activated molecular sieves (2 Å). AIBN was re-crystallized from methanol.

Characterization methods

^{1}H-, ^{13}C-, ^{19}F-, and DOSY-NMR spectra were measured with an Agilent Technologies 400 MHz VNMRS (400 MHz) in deuterated solvents like CDCl$_3$ and D$_2$O and analyzed with
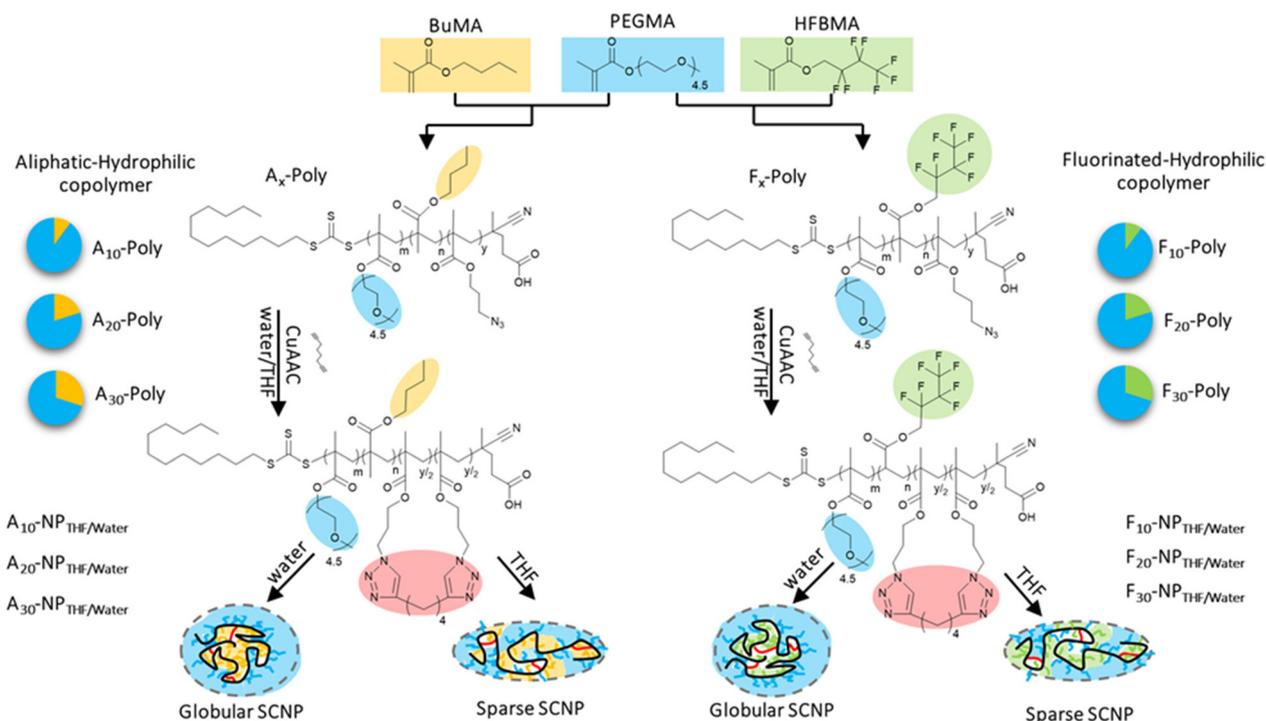
Scheme 1 Synthesis of random copolymers from three different methacrylate monomers. Each polymer type displays two different philicities and is produced in three different molar compositions. Crosslinking after single chain collapse generates the desired single chain nanoparticles (SCNPs) with the desired compartments.

MestReNova 14.2.1-27684 from Mestrelab Research S.L. SEC measurements were performed at 30 °C on a Viscotek GPCmax VE 2001 from Malvern applying a CLM3008 precolumn and a CLM3008 main column with 3.0 mg mL^{-1} sample concentration. ESI-ToF spectroscopy measurements were performed on an ESI-quadrupole time-of-flight mass spectrometer system (compact LC-MS system) from Bruker Daltonics GmbH & Co. KG with sample concentration 0.1–0.3 mg ml^{-1} in methanol. Attenuated total reflection-infrared (ATR-FTIR) spectroscopy measurements were done on a Bruker Tensor VERTEX 70 spectrometer equipped with a golden gate unit and the software Opus 8.2 was used to analyze the spectra. AFM imaging was performed on mica surfaces using a Nanosurf CoreAFM with Tap190AI-G cantilevers in the phase-contrast mode. Turbidimetry measurements were done using a JASCO J-1500 with a PTC-510 cell holder at 400 nm with fixed sample concentration of 1.0 mg mL^{-1}. Absorption measurements were conducted on a UV/Vis spectrometer from PerkinElmer at room temperature. Fluorescence measurements were performed using a Cary Eclipse Fluorescence Spectrometer from Agilent using Hellma Analytics quartz 10 mm glass cuvettes at room temperature. CW EPR measurements were conducted using a Miniscope MS 5000 (Magnettech GmbH, Berlin, and Freiberg Instruments, Freiberg, Germany) in water at 25 °C and the simulations were done using Matlab (The Mathworks, Inc.) in combination with the EasySpin program. The fluorescence quantum yields (φ_f) were determined in aqueous solutions at room temperature (25 μM) with a 405 nm ps laser

diode driven at 20 MHz (LDH-405, Picoquant, Berlin). Decay associated spectra (DAS) were determined from time- and wavelength-correlated fluorescence data performed with a setup as described in ref. 34 and 35 (see the ESI†).

Synthesis of random copolymers A$_x$-poly

AIBN ($\approx$1 mmol equivalent), the chain-transfer agent CDPA ($\approx$5 mmol equivalent), PEGMA (1 mol equivalent), BuMA and APMA (see Table S1 in the ESI†) were dissolved in dry DMSO (c = 3.3 M). The reaction mixture was purified of oxygen *via* 5 freeze–pump–thaw cycles. Subsequently, the reaction was carried out for 3 hours at 70 °C. The reaction was quenched using an ice bath. The polymer solution was transferred for dialysis in water for three days using dialysis tubes with 5 kDa molecular weight cutoff, followed by an additional 3 days of dialysis in THF. The copolymers were characterized using SEC in THF and ^{1}H-NMR in CDCl$_3$ (see Scheme 1, Table 1 and Table S1 in the ESI†).

^{1}H NMR (400 MHz, CDCl$_3$, δ in ppm): 0.84–0.99 (–CH$_3$ protons of the backbone, 3H), 1.21–1.85 (–CH$_2$– protons of the backbone, 2H), 3.51–3.62 (–O-CH$_2$-CH$_2$-O– protons of PEGMA, 4H), 3.34 (–O-CH$_3$ protons of PEGMA, 3H), 3.38 (–COO-CH$_2$– protons of APMA, 2H), 3.90 (–COO-CH$_2$– protons of BuMA, 2H) and 4.04 (–COO-CH$_2$– protons of PEGMA, 2H).

Synthesis of random copolymers F$_x$-poly

AIBN ($\approx$1 mmol equivalent), the chain-transfer agent CDPA ($\approx$5 mmol equivalent), PEGMA (1 mol equivalent), HFBMA and

Table 1 Collected data for the precursor polymers and their respective SCNPs: monomer compositions, (apparent) molecular weight $M_{n,app}$, polydispersity index PDI, compaction factor G, hydrodynamic radius r_h as determined from DOSY-NMR spectra, and cloud point temperature T_{cp} as determined from turbidimetry

Sample	$m:n:y$[a]	$M_{n,app}$[b]/ kDa	PDI[a]	G[c]	r_h[d]/ nm	T_{cp}[e]/ °C	Sample	$m:n:y$[a]	$M_{n,app}$[b]/ kDa	PDI[a]	G[c]	r_h[d]/ nm	T_{cp}[e]/ °C
A_{10}-poly	79:11:10	14.6	1.2	—	4.0	50	F_{10}-poly	79:9:12	15.5	1.3	—	4.1	48
A_{10}-NP$_{water}$		7.9	1.2	46%	5.8	55	F_{10}-NP$_{water}$		9.5	1.3	40%	5.6	58
A_{10}-NP$_{THF}$		11.4	1.2	22%	3.3	56	F_{10}-NP$_{THF}$		12.3	1.3	21%	3.7	62
A_{20}-poly	69:20:10	14.6	1.3	—	3.4	43	F_{20}-poly	71:19:9	17.1	1.4	—	3.5	42
A_{20}-NP$_{water}$		10.8	1.5	26%	4.9	45	F_{20}-NP$_{water}$		11.3	1.3	34%	5.5	44
A_{20}-NP$_{THF}$		13.2	1.3	10%	2.5	53	F_{20}-NP$_{THF}$		10.8	1.5	37%	3.1	45
A_{30}-poly	62:27:10	17.0	1.3	—	3.6	38	F_{30}-poly	61:30:9	19.0	1.5	—	4.2	35
A_{30}-NP$_{water}$		9.1	1.7	46%	4.0	44	F_{30}-NP$_{water}$		10.0	1.6	47%	5.0	43
A_{30}-NP$_{THF}$		17.0	1.5	0%	3.2	40	F_{30}-NP$_{THF}$		17.8	2.0	11%	3.7	44

[a] Molar ratio of PEGMA : BuMA : APMA in A_x-poly and of PEGMA : HFBMA : APMA in F_x-poly, analyzed from ^{1}H-NMR spectra in CDCl$_3$. [b] Measured by SEC in THF. [c] Calculated from the (apparent) molecular weights using $G = 100\%(M_{n,polymer} - M_{n,app,SCNP})/M_{n,polymer}$. [d] Calculated from ^{1}H-DOSY NMR measurements in D$_2$O using $r_h = (k_B \cdot T)/(6\pi \cdot \eta \cdot D)$. [e] Measured by turbidimetry, $T_{cp} = T$ at 90% transmission.

APMA (see Table S1 in the ESI†) were dissolved in dry DMSO (c = 3.3 M). The reaction mixture was purified from oxygen *via* 5 freeze–pump–thaw cycles. Subsequently, the reaction was carried out for 3 hours at 70 °C. The reaction was quenched using an ice bath. The polymer solution was transferred for dialysis in water for three days using dialysis tubes with 5 kDa molecular weight cutoff, followed by an additional 3 days of dialysis in THF. The copolymers were characterized using SEC in THF and ^{1}H- and ^{19}F-NMR in CDCl$_3$ (see Scheme 1, Table 1 and Table S1 in the ESI†).

^{1}H NMR (400 MHz, CDCl$_3$, δ in ppm): 0.82–1.03 (–CH$_3$ protons of the backbone, 3H), 1.21–1.89 (–CH$_2$– protons of the backbone, 2H), 3.50–3.65 (–O-CH$_2$-CH$_2$-O– protons of PEGMA, 4H), 3.33–3.37 (–O-CH$_3$ protons of PEGMA, 3H), 3.38–3.42 (–COO-CH$_2$– protons of APMA, 2H), 4.05–4.08 (–COO-CH$_2$– protons of PEGMA, 2H) and 4.38–4.42 (–COO-CH$_2$– protons of HFBMA, 2H).

Crosslinking reaction of A_x-poly and F_x-poly in water

Crosslinking reactions were conducted in an oxygen-free environment using copper(ɪ)-catalyzed alkyne–azide cycloaddition (CuAAC) click reaction with high dilutions (polymer solution concentration ≈10^{-6} M). The precursor polymer and octadiyne as crosslinker were dissolved in 20–25 mL dry THF. This solution was slowly added to the reaction solution *via* a syringe pump (1 mL h^{-1}). The reaction solution contained copper(ɪɪ) sulfate pentahydrate (CuSO$_4$·5H$_2$O, 0.5 mmol), PMDTA (2.0 mmol), and sodium ascorbate (7.6 mmol) in deionized water (250–300 mL). After complete addition of the polymer solution, the product (A_x-NP$_{water}$ or F_x-NP$_{water}$) was extracted with DCM, dissolved in THF and purified by dialysis. The nanoparticles were characterized using SEC in THF and ^{1}H- and ^{19}F-NMR in CDCl$_3$ (see Scheme 1, Table 1 and Table S1 in the ESI†).

^{1}H NMR (400 MHz, CDCl$_3$, δ in ppm): 0.85–1.04 (–CH$_3$ protons of the backbone, 3H), 1.24–1.85 (–CH$_2$– protons of the backbone, 2H), 3.33–3.39 (–O-CH$_3$ protons of PEGMA, 3H), 3.54–3.67 (–O-CH$_2$-CH$_2$-O– protons of PEGMA, 4H), 3.94 (–COO-CH$_2$– protons of BuMA, 2H), 4.05–4.08 (–COO-CH$_2$– protons of PEGMA, 2H) and 4.38–4.42 (–COO-CH$_2$– protons of HFBMA, 2H).

Crosslinking reaction of A_x-poly and F_x-poly in THF

Crosslinking reactions were conducted in a water and oxygen-free environment using copper(ɪ)-catalyzed alkyne–azide cycloaddition (CuAAC) click reaction with high dilution (polymer solution concentration ≈10^{-6} M). The precursor polymer and octadiyne as crosslinker were dissolved in 20–25 mL dry THF. This solution was slowly added to the reaction solution *via* a syringe pump (1 mL h^{-1}). The reaction mixture contained copper(ɪ) bromide (CuBr, 0.4–0.5 mmol) and 2,2′-bipyridine (1.3 mmol) dissolved in dry THF (250–300 mL). After complete addition of the polymer solution, water was added and the product (A_x-NP$_{THF}$ or F_x-NP$_{THF}$) was extracted with DCM, dissolved in THF and purified by dialysis. The nanoparticles were characterized using SEC in THF and ^{1}H- and ^{19}F-NMR in CDCl$_3$ (see Scheme 1, Table 1 and Table S1 in the ESI†).

^{1}H NMR (400 MHz, CDCl$_3$, δ in ppm): 0.82–1.05 (–CH$_3$ protons of the backbone, 3H), 1.24–2.17 (–CH$_2$– protons of the backbone, 2H), 3.33–3.39 (–O-CH$_3$ protons of PEGMA, 3H), 3.53–3.66 (–O-CH$_2$-CH$_2$-O– protons of PEGMA, 4H), 3.94 (–COO-CH$_2$– protons of BuMA, 2H), 4.05–4.09 (–COO-CH$_2$– protons of PEGMA, 2H) and 4.42 (–COO-CH$_2$– protons of HFBMA, 2H).

Results and discussion

Design and synthesis strategy

The amphiphilic polymers and resulting SCNPs were designed and synthesized to balance the influence of their solvophilicity

on the resulting nanostructure and physicochemical behavior. The use of the aliphatic monomer *n*-butyl methacrylate (BuMA) in the A_x-poly copolymer and the fluorinated monomer 2,2,3,3,4,4,4-heptafluorobutyl methacrylate (HFBMA) in the F_x-poly copolymer allowed to generate polymers and SCNPs with varying hydrophobic strengths, as depicted in Scheme 1. The design of the two major types of random copolymers (A_x-poly and F_x-poly) was motivated to investigate the segregation between aliphatic and fluorinated side chains in view of compartment formation, as well as their impact on loading/binding to the hydrophobic compartments upon SCNP formation. The precursor polymers were synthesized as random copolymers by reversible-addition–fragmentation chain-transfer (RAFT) polymerization. The monomer feeds used mixtures of the hydrophilic poly(ethylene glycol)methyl ether methacrylate (PEGMA, M_n = 300 g mol^{-1}, DP_{PEG} = 4.5), either BuMA or HFBMA as hydrophobic entities, and azidopropyl methacrylate (APMA) as the crosslinking unit. Six different precursor random copolymers were designed that differ in their hydrophobic/hydrophilic molar composition, namely: 10 mol% aliphatic (A_{10}-poly), 20 mol% aliphatic (A_{20}-poly), 30 mol% aliphatic (A_{30}-poly), 10 mol% fluorinated (F_{10}-poly), 20 mol% fluorinated (F_{20}-poly) and 30 mol% fluorinated (F_{30}-poly) monomers (see Scheme 1). Monomer conversion ranged between 20 and 40% with resulting molecular weights varying from 15 to 19 kg mol^{-1} and PDI values between 1.2 and 1.5, as indicated by ^{1}H-NMR spectroscopy and SEC in THF (see Table 1). In addition, all polymers carry a third methacrylate monomer (APMA) with an azide group (–N$_3$) as a crosslinking site in amounts of 9–12 mol% in the final chains. The compositions of the final polymers (see Table 1) are in line with the initial feed ratios as proven by ^{1}H-NMR spectroscopy.

The copolymers were then probed for the preparation of the SCNPs to study collapse and crosslinking of the copolymer chains in different solvents. As the chain conformation and folding is based on the delicate solvent/polymer interactions, dependent on the ratio of hydrophobicity/hydrophilicity in the copolymer, two different routes were used: (I) crosslinking in a selective solvent (water), which is a good solvent for the PEGMA monomer and a nonsolvent for the hydrophobic monomers (BuMA and HFBMA); and (II) in a nonselective solvent (THF), which is a good solvent for all monomers. Subsequently the produced morphologies were preserved by covalent crosslinking through copper-catalyzed azide–alkyne click-reactions (CuAAC) since this method has proven its efficacy in producing SCNPs.[26,27,36,37] All six types of precursor copolymers display on average 5–7 crosslinking sites, provided by the presence of the azide functional group (–N$_3$) from the monomer APMA. The crosslinking process was designed to guarantee intrachain crosslinking and avoid multiple chain interactions by using the continuous addition procedure, in which the precursor polymers together with the external crosslinker (octadiyne) were slowly added to the crosslinking solution *via* a syringe pump. Thus, the final shape and size of the SCNPs as well as the formation of compartments within the SCNPs are dependent on the folding process of the single precursor polymer chains, which is influenced by polymer/solvent interactions, and on the chemical composition. Twelve different types of SCNPs were produced and reported, namely: A_{10}-NP$_{water}$, A_{20}-NP$_{water}$ and A_{30}-NP$_{water}$ from A_x-poly crosslinked in water; A_{10}-NP$_{THF}$, A_{20}-NP$_{THF}$ and A_{30}-NP$_{THF}$ from A_x-poly crosslinked in THF; F_{10}-NP$_{water}$, F_{20}-NP$_{water}$ and F_{30}-NP$_{water}$ from F_x-poly crosslinked in water; F_{10}-NP$_{THF}$, F_{20}-NP$_{THF}$ and F_{30}-NP$_{THF}$ from F_x-poly crosslinked in THF (see Scheme 1).

Size determination

After crosslinking the SCNPs their size was investigated using size exclusion chromatography (SEC), which reflected a change in the apparent molecular weights of the precursor copolymers and their corresponding SCNPs. In addition to size changes as determined by changes in the hydrodynamic radius (r_h) we used ^{1}H-DOSY-NMR to determine the size of the SCNPs. ATR-IR spectroscopy was used for each polymer before and after crosslinking to identify the vibrational band of the azide functional group (–N$_3$) from the monomer APMA around 2100 cm^{-1}, indicative of the progress of the crosslinking chemistry.[38] In all cases after crosslinking no presence of the vibrational band at 2100 cm^{-1} for the SCNPs was observed. This indicates a complete crosslinking by formation of the 1,2,3-triazole ring and thus stabilization of the SCNPs can be assumed. This observation is supported through ATR-IR spectra of F_{30}-poly and its corresponding SCNPs (F_{30}-NP$_{THF/water}$) and A_{30}-poly and its corresponding SCNPs (A_{30}-NP$_{THF/water}$) (see Fig. 1a and Fig. S1 in the ESI†). Further, ^{1}H-NMR spectra for the SCNPs were inspected for the presence of the protons of any potentially unreacted alkyne groups (≡CH) at a chemical shift of 1.92 ppm and they showed no presence. In conclusion, the functional groups of azide (–N$_3$)
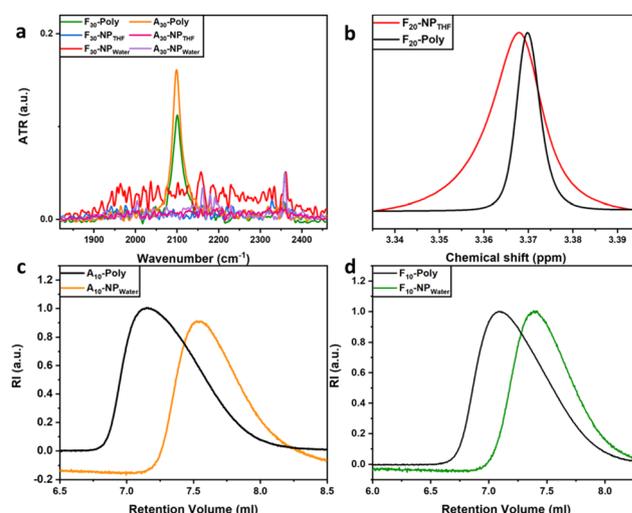
**Fig. 1** (a) ATR-IR absorption spectra for F_{30}-poly, F_{30}-NP$_{THF/water}$, A_{30}-poly and A_{30}-NP$_{THF/water}$. (b) ^{1}H-NMR spectra in CDCl$_3$ of F_{20}-poly (black) and F_{20}-NP$_{THF}$ (red). SEC curves in THF for (c) A_{10}-poly and A_{10}-NP$_{water}$ and (d) F_{10}-poly and F_{10}-NP$_{water}$.

and alkyne (≡CH) were completely consumed in CuAAC click-reactions to produce 1,2,3-triazole rings, part of the crosslinker, with on average 3 crosslinkers per SCNP. In addition, ^{1}H-NMR spectroscopy shows a broadening of the SCNPs' spectra due to restricted mobility of the copolymer side chains when compared with the spectra of the corresponding precursor polymers.[39,40] Full width at half-maximum (FWHM) analysis at 3.37 ppm, which corresponds to the chemical shift of –O-CH$_3$ of PEG in F$_{20}$-poly and F$_{20}$-NP$_{THF}$, shows an example with 6.1 mHz and 14 mHz, respectively (see Fig. 1b, and Table S2 and Fig. S2, S6 and S7 in the ESI†).s

SEC is a commonly used method to investigate successful SCNP formation through reduced hydrodynamic volumes for the SCNPs when compared to the respective precursor polymers.[41,42] For all copolymer species, the peaks of the precursor polymers appear at lower retention volumes than the ones corresponding to the SCNPs, indicating the reduction of the hydrodynamic volumes due to successful collapse/crosslinking.[43] This behavior is observed in all SCNPs and their respective precursor polymers (see Fig. 1c, d and Fig. S10 in the ESI†). The compaction factor (G) is an indication of the compactness of the SCNP after undergoing intramolecular covalent crosslinking. It's a direct insight into the size change and a relative quantification using the molecular weights of the precursor copolymer chains and the apparent molecular weights of the corresponding SCNPs attained from SEC. All SCNPs show up to 47% compaction in comparison with their corresponding precursor copolymers (see Table 1). Further, the general trend shows that SCNPs crosslinked in water show higher compactions than those crosslinked in THF. This sup-ports the conclusion that the morphology produced in water is more globular and compact and the morphology produced in THF is rather loose and less compact, hence resulting in sparse SCNPs.[37] Moreover, size determination measurements were carried out using ^{1}H-DOSY NMR in deuterated water (D$_2$O). The Stokes–Einstein equation (see Table 1) was employed to estimate the hydrodynamic radii, taking into account the temperature and the viscosity of the solvent during the measurement.[44] During folding and collapsing, the individual polymer chains undergo rearrangement due to intermolecular interactions (solvent/polymer) and intramolecular interactions (chain segments of the polymer), thus different behavior is expected for the collapse in different solvents. As an example, for the water-collapsed SCNPs, A$_{10}$-poly displays a r_h of 4.0 nm, while its corresponding nanoparticle A$_{10}$-NP$_{water}$ exhibits a r_h of 5.8 nm. All other sample pairs follow the same behavior (Fig. 2a), with increased r_h of the crosslinked SCNPs when compared to the corresponding precursor polymers. This indicates a larger solvation layer around the SCNPs, because of the internal structures which are formed during the single-chain collapse.[45] Since the chain has undergone folding and collapsing events this implies that the randomly-dispersed side chains of different philicities along the backbone are induced to rearrange due to intermolecular interactions (solvent–side chain) and intramolecular interactions (side chain–side chain) to end up with most of the hydrophilic side chains facing the solvent phase and hydrophobic side chains folded inside. Additionally, ^{1}H-DOSY NMR spectra were measured for those SCNPs which were crosslinked in THF. In contrast to the crosslinking behavior in
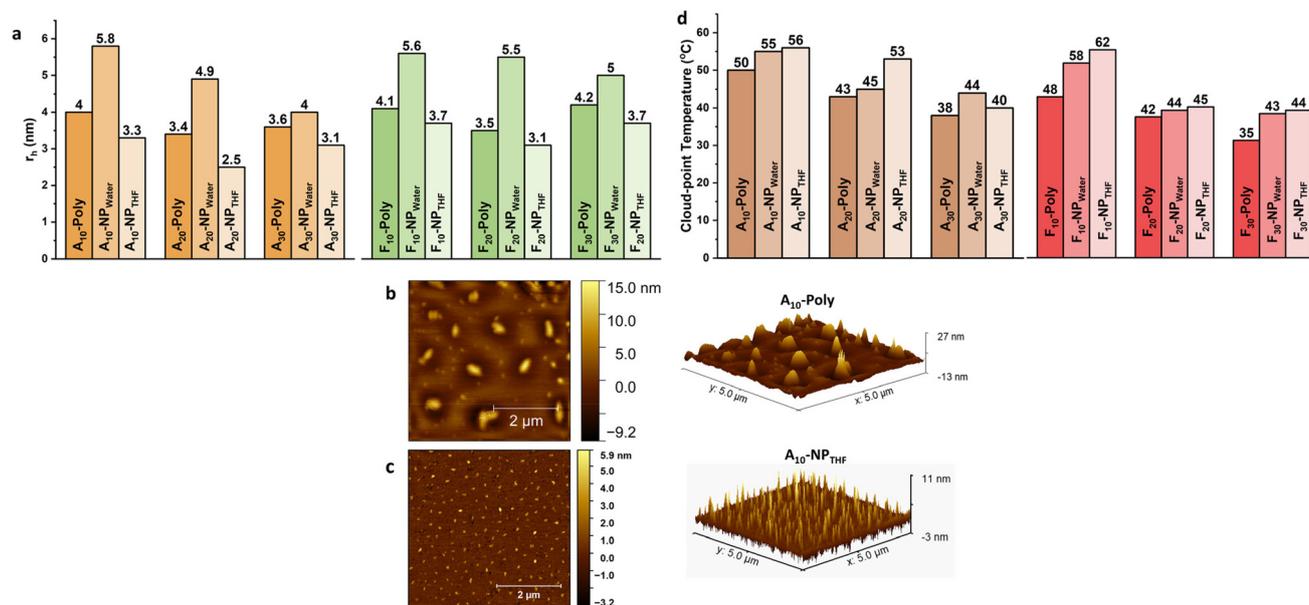

Fig. 2 (a) Hydrodynamic radii (nm) as reported from ^{1}H-DOSY NMR spectra in D$_2$O for A$_x$-poly and the corresponding nanoparticles (A$_x$-NP$_{water/THF}$) and F$_x$-poly and its corresponding nanoparticles (F$_x$-NP$_{water/THF}$) crosslinked in water and in THF. AFM images of (b) A$_{10}$-poly and (c) A$_{10}$-NP$_{THF}$. (d) Cloud point temperatures, T_{cp} as determined from turbidimetry analysis for all copolymer species before and after crosslinking reactions in water and in THF.

water, for both species, A_x-NP$_{THF}$ and F_x-NP$_{THF}$, the size reduces but does not change drastically after crosslinking in THF. We assume that when SCNPs are formed in a nonselective solvent like THF, the arrangement of the monomers and their philicities take place locally and across the chain. Consequently, the resulting SCNPs exhibit a looser structure with separate local domains of different natures, rather than a core–shell globular structure. Instead, they adopt a sparse structure, resulting in a smaller solvation layer around the particle compared to SCNPs formed in water as a selective solvent. This is reflected in the behavior of the hydrodynamic radii which appear smaller in this case, as visible in Fig. 2a. It is worth mentioning that dynamic light scattering (DLS) measurements were conducted as a tool to observe size differences. After inspection of the data (Fig. S16 and Table S4†), it has been concluded that there are differences in r_h among the corresponding species when compared with those attained from [1]H-DOSY. This is possibly due to particle agglomeration happening during the DLS measurement, in addition to the challenging nature of the measured particles' size that pushes the DLS method and its accuracy to its limits. Nonetheless, a general trend has been noticed in DLS measurements that shows the precursor copolymers and their corresponding SCNPs are in the same size range. We have chosen to focus on [1]H-DOSY data since it offers more precision.[42] AFM imaging is used as an additional tool to navigate the conformation and size change due to the collapse and crosslinking events. The images show obvious changes in the measured heights of the detected particles deposited on mica surfaces. The dimensions of the SCNPs appear to be significantly smaller than the dimensions of the precursor polymer. In the case of the precursor polymer, A_{10}-poly, the average height of the scanned particles is 14.2 nm and for its corresponding SCNPs (A_{10}-NP$_{THF}$) the average height is 10.3 nm (see Fig. 2b and c, and Fig. S10 and S11 in the ESI†).

Thermal properties and core investigations

Turbidimetry was used to probe changes in solubility as a function of temperature by the thermo-responsive behavior of the poly(ethylene glycol)-side chains of the monomer PEGMA (see Scheme 1), constituting 70 to 90% mole fraction of the copolymers.[46] Cloud-point temperatures (T_{cp}) were observed at 90% transmittance of the aqueous solutions at a fixed concentration of 1.0 mg ml^{-1} for the precursor polymers as well as the SCNPs. All of the precursor copolymers and the corresponding SCNPs exhibited sharp LCST behavior at various temperatures (Fig. S18†). Precursor copolymer types A_{10}-poly and F_{10}-poly and the corresponding SCNPs exhibited the highest T_{cp}, due to the higher content of PEG side chains. All in all, the observed elevation of T_{cp} for all SCNPs in comparison with their precursor copolymer chains suggests enhanced solubility of the SCNPs upon stabilizing the folded structure with internal covalent crosslinking. Hence, the solubility is mainly dominated by the hydrophilic PEG chains, increasing the overall solubility in water. This effect is particularly pronounced in the samples that were crosslinked in THF, whose

resulting morphology after the collapse and crosslinking events in THF resembles a sparse structure. The compactness of the SCNPs can be described by the G factor. Hence, SCNPs formed in THF have a larger surface area compared to a sphere, leading to increased exposure to surrounding water molecules. The overall effect is reflected in higher solubility and correspondingly higher T_{cp} (see Fig. 2d). Additionally, it was noticed that the aliphatic SCNPs showed sharper LCST-type phase separation behavior in comparison with the fluorinated SCNPs (see Fig. S18†).

To delve deeper into the nature of the SCNPs derived from both types of copolymers and to probe philicity differences between the aliphatic and fluorophilic cores, decay associated spectra (DAS) were determined following the encapsulation of fluorescent dyes. The dye which was used for emission and absorption measurements is a modified version of Brooker's Merocyanine (BM), known for its unique solvatochromism behavior, which depends on the polarity of the surrounding media. Notably, it exhibits the highest energy absorption in water and the lowest in chloroform, accompanied by a color change from yellow to blue, respectively.[47,48] The modification of the dye involves attaching either an aliphatic chain (A-BM) or a fluorinated chain (F-BM) to reach the desired selectivity for each of the compartmeents. Further this modification aims to facilitate the diffusion of the dye molecule into either the aliphatic core or the fluorinated core of the nanoparticle. Overall by this modification the dye molecule will preferentially diffuse into the aliphatic compartment, the same principle applies to the dye with the fluorinated side chain. The technique has been previously employed by Delledonne et al.[28] and was now adapted for our system (see the ESI†) to check for the formation of internal compartments inside the SCNPs.

We focussed on the cores of the following SCNPs, A_{30}-NP$_{water}$ and F_{30}-NP$_{water}$. Absorption wavelengths for A-BM and F-BM when dissolved in water are 367 nm and 375 nm, respectively. Both dyes experience a red shift when encapsulated in the core of the SCNPs (A_{30}-NP$_{water}$ and F_{30}-NP$_{water}$). More precisely, A-BM shifts to 388 nm and 390 nm, respectively. F-BM shifts to 400 nm in both cores (see Table 2 and Fig. S15 in the ESI†).

Table 2 Collected data from DAS and absorption spectra for A-BM and F-BM

Species	Parameters	F-BM	A-BM
F_{30}-NP$_{water}$	λ/nm	400	390
	τ (black)/ps	118	77
	φ/%	2.2	1.8
A_{30}-NP$_{water}$	λ/nm	400	388
	τ (black)/ps	100	77
	φ/%	1.8	1.7
Water	λ/nm	375	367
	φ/%	0.7	0.7

λ: absorption wavelength. τ: fluorescence life-time of the dominant component (black). φ: fluorescence quantum yield.
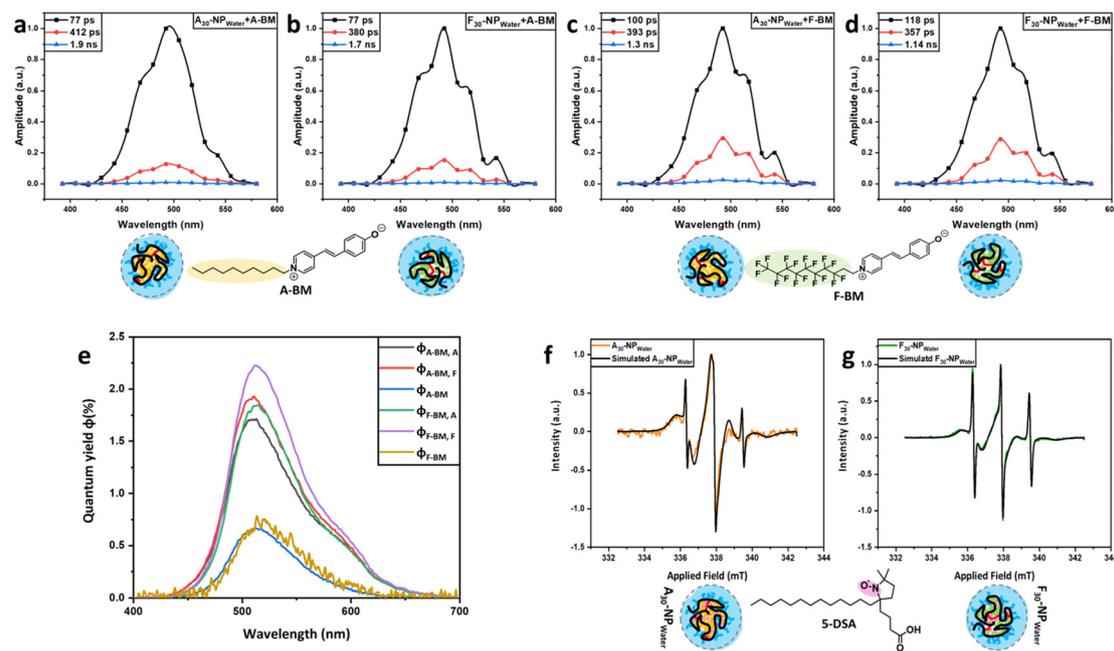
Fig. 3 DAS of A-BM in (a) A_{30}-NP_{water} and (b) F_{30}-NP_{water}; DAS of F-BM in (c) A_{30}-NP_{water} and (d) F_{30}-NP_{water}. (e) Emission spectra of A-BM and F-BM. CW-EPR spectra and simulations of 5-DSA in the core of (f) A_{30}-NP_{water} and (g) F_{30}-NP_{water}.

DAS shows three different fluorescence components (see Fig. 3a–d). The dominating fluorescence component (black) for A-BM in A_{30}-NP_{water} and F_{30}-NP_{water} experiences the shortest life-time (77 ps) when compared with F-BM in A_{30}-NP_{water} (100 ps) and the longest life-time in F_{30}-NP_{water} (118 ps). This correlates with the highest quantum yield observed for F-BM in F_{30}-NP_{water} (2.2%) and indicates that F-BM exhibits reduced quenching by water molecules in the fluorinated core. This is reasoned by the higher affinity of F-BM in the F_{30}-NP_{water} core in comparison to the A_{30}-NP_{water} core. The second fluorescence component (red) has the longest life-time (412 ps) when A-BM is encapsulated in the aliphatic core of A_{30}-NP_{water} possibly indicating a stronger affinity of A-BM towards the aliphatic core than the fluorinated core of F_{30}-NP_{water}. The third fluorescence component (1.1–1.9 ns, blue) is very small in amplitude and therefore not further evaluated. Fluorescence spectra of A-BM and F-BM in both cores were normalized to the corresponding quantum yields at 25 °C in aqueous solutions (see Fig. 3e and Table 2). The quantum yields $\varphi_{A/F-BM}$ of both dyes in water, which in their added amounts are equal to 0.7%,[48] were used to calculate the relative quantum yields of the dyes when encapsulated in A_{30}-NP_{water} and F_{30}-NP_{water} cores, $\varphi_{A/F-BM, A}$ and $\varphi_{A/F-BM, F}$, respectively. The quantum yields $\varphi_{A-BM, A}$, $\varphi_{A-BM, F}$ and $\varphi_{F-BM, A}$ show comparable and higher values compared with φ_{F-BM} and φ_{A-BM} in water (1.7%–1.8%). The highest quantum yield was recorded for F-BM in the fluorinated core, $\varphi_{F-BM, F}$ = 2.2%, clearly indicating that fluorescence quenching is most strongly suppressed in a fluorinated environment when compared with an aliphatic environment. Further investigations targeting the cores of A_{30}-NP_{water} and F_{30}-NP_{water} were carried out using the potential of continu-

ous wave electron paramagnetic resonance (CW-EPR) spectroscopy, relying on a spin-labeled fatty acid, 5-doxyl-stearic acid (5-DSA), expected to specifically probe the hydrophobic cores of the SCNPs. Subsequently, CW-EPR spectra simulations were applied to identify the amount of bound 5-DSA within the SCNPs, as well as the strength of these bonds, by analyzing the inhibited motion of the bound spin probe.[49] The CW-EPR spectra represent the sum of all paramagnetic signals inside the SCNP solutions, originating from two components: (I) freely solvated and rotating 5-DSA, and (II) SCNP-bound 5-DSA molecules. It was observed that the aliphatic SCNPs which were crosslinked in water (A_{30}-NP_{water}) exhibit a higher binding capacity towards hydrophobic molecules like 5-DSA. For a SCNP/5-DSA ratio of 2/1, more than 96% of the 5-DSA molecules are located within the core of A_{30}-NP_{water}. The core of F_{30}-NP_{water} merely captures approximately 88% of the spin probe. Hence, the aliphatic probe has a higher affinity to be bound to the aliphatic core of A_{30}-NP_{water} than to the fluorinated core of F_{30}-NP_{water}. Furthermore, the rotation correlation time of SCNP-bound 5-DSA amounts to 7.59 ns. This value is identical for both cores of A_{30}-NP_{water} and F_{30}-NP_{water} and is higher than that of the free 5-DSA in water (0.10–0.18 ns), caused by the strong encapsulation of 5-DSA in the SCNP cores, decreasing its individual movement (see Fig. 3f and g, and Fig. S13 and Table S3 in the ESI†).

Conclusion

We here investigated the structural and physicochemical differences caused by segregation of hydrophobic and fluorophilic

parts inside an amphiphilic single chain nanoparticle, SCNPs to generate internal nanosized compartments therein. Two sets of random amphiphilic copolymers were synthesized as precursor polymers, containing either hydrophilic–aliphatic or hydrophilic–fluorophilic monomers, and subsequently subjected to single-chain collapse, either in water as a selective solvent, or in THF as a nonselective solvent. The hydrophobic/hydrophilic ratio was systematically varied across the two types of the copolymers in three different hydrophobic molar compositions: 30 mol%, 20 mol% and 10 mol% in the final polymers. We explored the impact of changing this ratio on the final shape and morphology of the produced SCNPs and thus could reveal the formation of internal hydrophobic/fluorophilic cores resulting from the collapse and intra-chain crosslinking of copolymer chains in a selective solvent like water. Both EPR spectroscopy and fluorescence spectroscopy (DAS) indicated a clear difference of the formed SCNPs in different collapsing media and indicate the formation of water soluble SCNPs from random polymer chains with different philicity-distributions inside the SCNPs. When an amphiphilic random polymer is collapsed and crosslinked in a selective solvent like water, the resulting morphology is a more globular, core–shell arrangement inside the SCNP. Conversely, when the same random polymer is crosslinked in a nonselective solvent like THF, it forms a sparse structure, with the different philicities distributed locally. The presented methods allow to generate two different types of SCNPs from the same precursor polymer chain based on the choice of the collapsing solvent, and a tuning of the compartments inside the corresponding SCNP, thus forming a novel approach to modulate the SCNPs' inner and outer structures – an important prerequisite for further exploitation of their function as catalysts and nanoreactors. An investigation aimed at elucidating the nature of the hydrophobic cores (aliphatic or fluorinated) was conducted by using DAS and CW-EPR spectroscopy of specifically labelled reported molecules, selective for either the hydrophobic or the fluorophilic compartment inside the SCNPs. Both methods showed that the choice of the type of hydrophobicity (aliphatic or fluorophilic) has influence on specifically locating small molecules inside parts of the SCNP cores. Hence, fluorinated molecules have a higher affinity to the fluorinated compartments, and aliphatic molecules to aliphatic compartments. This finding is important for the applications of SCNPs, *e.g.* in terms of drug delivery and selective catalysis, wherein an enzyme-like behavior can be reached *via* sleective compartmentation behavior. Herein even small differences in binding affinities can have major influences on the efficiency of the release of small substrate- or drug molecules, located inside the specific compartments, and released upon external triggers, such as NIR-activation or photoacoustic responses.

Conflicts of interest

There are no conflicts to declare.

Acknowledgements

References

1 D. B. Varshey, J. R. G. Sander, T. Friščić and L. R. MacGillivray, in *Supramolecular Chemistry*, 2012.

2 S. Förster and T. Plantenberg, *Angew. Chem., Int. Ed.*, 2002, **41**, 688–714.

3 C. L. D. Gibb and B. C. Gibb, in *Supramolecular Chemistry*, 2012.

4 S. Chen, B.-D. Lechner, A. Meister and W. H. Binder, *Nano Lett.*, 2016, **16**, 1491–1496.

5 D. Heinz, E. Amado and J. Kressler, *Polymers*, 2018, **10**, 960.

6 Y. Mai and A. Eisenberg, *Chem. Soc. Rev.*, 2012, **41**, 5969–5985.

7 T. Terashima, T. Mes, T. F. A. De Greef, M. A. J. Gillissen, P. Besenius, A. R. A. Palmans and E. W. Meijer, *J. Am. Chem. Soc.*, 2011, **133**, 4742–4745.

8 A. Sanchez-Sanchez, A. Arbe, J. Kohlbrecher, J. Colmenero and J. A. Pomposo, *Macromol. Rapid Commun.*, 2015, **36**, 1592–1597.

9 Y. Liu, S. Pujals, P. J. M. Stals, T. Paulöhrl, S. I. Presolski, E. W. Meijer, L. Albertazzi and A. R. A. Palmans, *J. Am. Chem. Soc.*, 2018, **140**, 3423–3433.

10 J. Rubio-Cervilla, E. Gonzalez and J. A. Pomposo, *Nanomaterials*, 2017, **7**, 341–360.

11 M. Artar, E. R. J. Souren, T. Terashima, E. W. Meijer and A. R. A. Palmans, *ACS Macro Lett.*, 2015, **4**(10), 1099–1103.

12 M. A. J. Gillissen, I. K. Voets, E. W. Meijer and A. R. A. Palmans, *Polym. Chem.*, 2012, **3**, 3166–3174.

13 A. Latorre-Sanchez and J. A. Pomposo, *Chem. Commun.*, 2015, **51**, 15736–15738.

14 A. B. Benito, M. K. Aiertza, M. Marradi, L. Gil-Iceta, T. S. Zahavi, B. Szczupak, M. Jimenez-Gonzalez, T. Reese, E. Scanziani, L. Passoni, M. Matteoli, M. D. Maglie, A. Orenstein, M. Oron-Herman, G. Kostenich, L. Buzhansky, E. Gazit, H. J. Grande, V. Gomez-Vallejo, J. Llop and I. Loinaz, *Biomacromolecules*, 2016, **17**, 3213–3221.

15 A. P. P. Kröger, N. M. Hamelmann, A. Juan, S. Lindhoud and J. M. J. Paulusse, *ACS Appl. Mater. Interfaces*, 2018, **10**, 30946–30951.

16 Y. Yang, Y. Li, Q. Lin, C. Bao and L. Zhu, *ACS Macro Lett.*, 2016, **5**, 301–305.

17 A. P. P. Kröger and J. M. J. Paulusse, *J. Controlled Release*, 2018, **286**, 326–347.

18 J. A. Pomposo, I. Perez-Baena, F. Lo Verso, A. J. Moreno, A. Arbe and J. Colmenero, *ACS Macro Lett.*, 2014, **3**, 767–772.

19 A. J. Moreno, F. Lo Verso, A. Arbe, J. A. Pomposo and J. Colmenero, *J. Phys. Chem. Lett.*, 2016, **7**, 838–844.

20 E. Verde-Sesto, A. Arbe, A. J. Moreno, D. Cangialosi, A. Alegría, J. Colmenero and J. A. Pomposo, *Mater. Horiz.*, 2020, **7**, 2292–2313.

21 S. Liao, L. Wei, L. A. Abriata and F. Stellacci, *Macromolecules*, 2021, **54**, 11459–11467.

22 R. Upadhya, N. S. Murthy, C. L. Hoop, S. Kosuri, V. Nanda, J. Kohn, J. Baum and A. J. Gormley, *Macromolecules*, 2019, **52**, 8295–8304.

23 S. Mavila, O. Eivgi, I. Berkovich and N. G. Lemcoff, *Chem. Rev.*, 2016, **116**, 878–961.

24 G. M. t. Huurne, A. R. A. Palmans and E. W. Meijer, *CCS Chem.*, 2019, **1**, 64–82.

25 A. Nitti, R. Carfora, G. Assanelli, M. Notari and D. Pasini, *ACS Appl. Nano Mater.*, 2022, **5**, 13985–13997.

26 J. F. Hoffmann, A. H. Roos, F.-J. Schmitt, D. Hinderberger and W. H. Binder, *Angew. Chem., Int. Ed.*, 2021, **60**, 7820–7827.

27 J. F. Thümmler, A. H. Roos, J. Krüger, D. Hinderberger, F.-J. Schmitt, G. Tang, F. G. Golmohamadi, J. Laufer and W. H. Binder, *Macromol. Rapid Commun.*, 2023, **44**, 2200618.

28 A. Delledonne, E. Guazzelli, S. Pescina, A. Bianchera, G. Galli, E. Martinelli and C. Sissa, *ACS Appl. Nano Mater.*, 2023, **6**(17), 15551–15562.

29 J. H. Ko, A. Bhattacharya, T. Terashima, M. Sawamoto and H. D. Maynard, *J. Polym. Sci., Part A: Polym. Chem.*, 2019, **57**, 352–359.

30 Y. Koda, T. Terashima, M. Sawamoto and H. D. Maynard, *Polym. Chem.*, 2015, **6**, 240–247.

31 Y. Koda, T. Terashima and M. Sawamoto, *Macromolecules*, 2016, **49**, 4534–4543.

32 M. Matsumoto, M. Sawamoto and T. Terashima, *ACS Macro Lett.*, 2019, **8**, 320–325.

33 M. Shibata, M. Matsumoto, Y. Hirai, M. Takenaka, M. Sawamoto and T. Terashima, *Macromolecules*, 2018, **51**, 3738–3745.

34 F. J. Schmitt, E. G. Maksimov, P. Hätti, J. Weißenborn, V. Jeyasangar, A. P. Razjivin, V. Z. Paschenko, T. Friedrich and G. Renger, *Biochim. Biophys. Acta, Bioenerg.*, 2012, **1817**, 1461–1470.

35 F. J. Schmitt, E. G. Maksimov, H. Suedmeyer, V. Jeyasangar, C. Theiss, V. Z. Paschenko, H. J. Eichler and G. Renger, *Photonics Nanostruct.*, 2011, **9**, 190–195.

36 S. Neumann, M. Biewend, S. Rana and W. H. Binder, *The CuAAC: Principles, Homogeneous and Heterogeneous Catalysts, and Novel Developments and Applications*, report 1022-1336, 2020.

37 J. F. Thümmler, R. Maragani, F.-J. Schmitt, G. Tang, S. M. Rahmanlou, J. Laufer, H. Lucas, K. Mäder and W. H. Binder, *Chem. Commun.*, 2023, **59**, 11373–11376.

38 X. S. Gai, B. A. Coutifaris, S. H. Brewer and E. E. Fenlon, *Phys. Chem. Chem. Phys.*, 2011, **13**, 5926–5930.

39 T. Terashima, T. Sugita, K. Fukae and M. Sawamoto, *Macromolecules*, 2014, **47**, 589–600.

40 K. Akiyoshi, S. Deguchi, N. Moriguchi, S. Yamaguchi and J. Sunamoto, *Macromolecules*, 1993, **26**, 3062–3068.

41 O. Altintas and C. Barner-Kowollik, *Macromol. Rapid Commun.*, 2016, **37**, 29–46.

42 E. Blasco, B. T. Tuten, H. Frisch, A. Lederer and C. Barner-Kowollik, *Polym. Chem.*, 2017, **8**, 5845–5851.

43 J. Engelke, J. Brandt, C. Barner-Kowollik and A. Lederer, *Polym. Chem.*, 2019, **10**, 3410–3425.

44 Y. Cohen, L. Avram and L. Frish, *Angew. Chem., Int. Ed.*, 2005, **44**, 520–554.

45 H. Zhang, L. Zhang, J. You, N. Zhang, L. Yu, H. Zhao, H.-J. Qian and Z.-Y. Lu, *CCS Chem.*, 2021, **3**, 2143–2154.

46 A. Gandhi, A. Paul, S. O. Sen and K. K. Sen, *Asian J. Pharm. Sci.*, 2015, **10**, 99–107.

47 V. Z. Shirinian and A. A. Shimkin, in *Heterocyclic Polymethine Dyes*, ed. L. Strekowski, Springer Berlin Heidelberg, Berlin, Heidelberg, 2008, ch. 110, pp. 75–105.

48 V. Cavalli, D. C. da Silva, C. Machado, V. G. Machado and V. Soldi, *J. Fluoresc.*, 2006, **16**, 77–86.

49 P. D. Martin, B. Svensson, D. D. Thomas and S. Stoll, *J. Phys. Chem. B*, 2019, **123**, 10131–10141.